WOOD MATERIAL SCIENCE & ENGINEERING
2023, VOL. 18, NO. 3, 1076–1085
https://doi.org/10.1080/17480272.2022.2106447

Taylor & Francis
Taylor & Francis Group

Check for updates

Physical and mechanical properties of the cement composite with makino bamboo fibers disintegrated by alkali treatment

Teng-Chun Yang [a], Zai-Shin Hua[b] and Hsuan-Teh Hu [b,c]

[a]Department of Forestry, National Chung Hsing University, Taichung, Taiwan; [b]Department of Civil Engineering, National Cheng Kung University, Tainan, Taiwan; [c]Department of Civil and Disaster Prevention Engineering, National United University, Miaoli, Taiwan

ABSTRACT

In this study, disintegrated bamboo fibers (DBFs) were extracted from alkali-treated makino bamboo sticks (BSs). The chemical compositions and tensile properties of DBFs were investigated using Fourier transform infrared (FTIR), X-ray diffraction (XRD), thermogravimetric (TG) analysis, and tensile tests. The results indicated that a change in functional groups, a reduction in the crystallinity index, and better thermal stability were observed for DBFs than for BSs. Regardless of the collapse of parenchyma cells and separation and twist of the fibers on the surface of the DBF, its average tensile strength and tensile modulus were 204 MPa, and 13 GPa, respectively. Additionally, DBFs were added into a cement matrix to fabricate bamboo fiber/cementitious composites (BCCs).

The apparent density and most of the mechanical properties of BCCs decreased when the addition of the DBFs increased above 1 wt%. However, the BCC with 1 wt% of DBFs showed the lowest drying shrinkage and a slight increase in the specific energy under tensile testing. Accordingly, the results showed that 1 wt% DBFs as an adequate content is proposed to be added into the cement.

ARTICLE HISTORY
Received 23 May 2022
Revised 21 July 2022
Accepted 23 July 2022

KEYWORDS
Alkali treatment; bamboo fiber; cement; makino bamboo

Introduction

Natural fiber/cement composites have attracted increasing attention in cement composite science. Many previous studies reported that natural fibers, such as sugarcane bagasse, sisal, hemp, jute, and bamboo, improve the mechanical strength and yield a high energy absorption capacity of cement composites (Li et al. 2006, Onesippe et al. 2010, Silva et al. 2010, Chakraborty et al. 2013, Sanchez-Echeverri et al. 2020). Additionally, the addition of natural fibers significantly enhances crack resistance and increases the impact resistance of the composites (Filho et al. 2005, Tonoli et al. 2013, Zhou et al. 2013, Xie et al. 2019). According to the previous studies described above, the variety of factors that affect the physical and mechanical properties of natural fiber/cement composites are as follows: (1) the nature of the matrix and mix design; (2) the casting and curing of composites; and (3) the type, modification, and characteristics of fibers.

Among natural fiber resources, bamboo as an additive is widely used in cement matrices due to its fast growth, biodegradability, and economical and eco-friendly properties. However, bamboo, which is a natural resource, has an intrinsic hydrophilic nature, resulting in high hygroscopicity and low compatibility between fibers and hydrophobic matrices. Several previous studies reported that chemical modifications, especially alkali treatment, can cause fibers with low hygroscopicity and increase fiber roughness, further strengthening the mechanical strength and fracture toughness of bamboo fiber/cement composites (BCCs) (Xie et al. 2015, Li et al. 2017, Xie et al. 2019, Sanchez-Echeverri et al. 2020, Sanchez-Echeverri et al. 2021). Li et al. (2017) investigated the properties of alkali-treated bamboo fiber (BF)-reinforced oil-well cementitious composites. The results demonstrated that increases in the thermal stability and roughness on the surface of BFs were observed after 10% alkali treatment. Additionally, the incorporation of 0.5 wt% alkali-treated BFs content increases the splitting tensile strength and flexural strength of the cement composite accompanied by a decrease in compressive strength. Sanchez-Echeverri et al. (2020) stated that the flexural strength and toughness of BCCs reinforced with $Ca(OH)_2$-treated BFs were higher than those of BCCs without and with untreated fibers. As mentioned by Sanchez-Echeverri et al. (2021), the findings indicated that the incorporation of *Guadua* fibers prepared by alkali treatment combined with mechanical refinement improved the flexural strength and specific energy of BCCs. Xie et al. (2015, 2019) reported that BCC with the optimal content of cellulosic fibers, which were isolated from bamboo, improved the flexural strength and fracture toughness by 24.3% and 45 times, respectively, while the absorbed energy of BCCs with 4–16 wt% BFs was 2–24 times higher than that of BCC without BFs.

To the best of our knowledge, there is still little information available on the investigations of the physical and mechanical properties of cement composites with bamboo fibers disintegrated by alkali treatment. Accordingly, the present study aimed to determine the functional groups, the crystallinity, thermal stability, morphology of the fiber

CONTACT Teng-Chun Yang tcyang.04@nchu.edu.tw; Department of Forestry, National Chung Hsing University, Taichung 402, Taiwan; Hsuan-Teh Hu hthu@ncku.edu.tw Department of Civil Engineering, National Cheng Kung University, Tainan 701, Taiwan.

© 2022 Informa UK Limited, trading as Taylor & Francis Group

surface, and tensile properties of disintegrated bamboo fibers (DBFs). Furthermore, the effects of the DBF content on the apparent density, drying shrinkage, and mechanical properties (tensile properties, flexural properties, and compressive properties) of BCCs were further investigated.

Materials and methods

Materials

A type I ordinary Portland cement (OPC) as a binder material, whose density is in the range of 2500–3300 kg/m^3, was purchased from Advaced-Tek Systems Co., Ltd. in Taiwan. Local river sand (Ligang Township, Taiwan) was used as fine aggregate, which had a content of particles less than 75 μm of 2.2% and a water-soluble chloride ion content of 0.0002%. Round bamboo sticks (BSs) with a diameter of 2 mm were obtained from 3-year-old makino bamboo (*Phyllostachys makinoi* Hayata) strips, as shown in Figure 1. Sodium hydroxide (NaOH) was purchased from Merck KGaA (Darmstadt, Germany).

Bamboo fiber disintegration

Disintegration of round BSs was performed by submerging and boiling them in the NaOH solution (concentration: 10%) in a digester at 100 °C for 3 h. The BSs were washed with distilled water after alkali treatment, and then DBFs were manually extracted from alkali-treated BSs. The length of the DBFs was cut and fixed at 20 mm (Figure 1).

Specimen preparation

The cement composites were prepared and cured according to CNS 3655 (2005). In the mix design for specimen preparation, the ratio of cement:sand was 1:3, and the water-cement ratio was kept at 0.5. Cement and water were mixed using a mechanical mixer (GF–201, Friend Food Machine Co., Ltd., Taiwan) to make a uniform slurry at a stirring speed of 146 rpm for 15 sec. Afterward, the required amount of sand was blended with the slurry at a stirring speed of 313 rpm for another 30 sec. The fresh mortar was cast immediately in various molds for test specimens. Additionally, the mortar specimens, which were set in the molds, were covered the plastic sheet for 24 h at ambient temperature (30 ± 2 °C). After setting, the specimens were removed from the molds and cured in saturated lime water for 28 days. For cement composites with bamboo fibers (BCCs), different mass fractions (1, 2, and 3 wt%) of DBFs were used to replace cement in the present study. To prevent the fibers from absorbing the required water content for BCCs, the DBFs were immersed in water for 24 h to obtain DBFs under saturated conditions. Before dropping sand, the saturated DBFs were blended into the cement slurry with stirring using a mechanical mixer. Other preparation procedures for BCCs were the same as those described above. The BCCs with 0, 1, 2, and 3 wt% DBF were designated BCC0, BCC1, BCC2, and BCC3, respectively.

Characteristics of bamboo fibers

The functional groups

Fourier transform infrared (FTIR) spectra of BSs and DBFs were measured on a Spectrum 100 FTIR spectrometer (Perkin Elmer, Buckinghamshire, UK) equipped with a MIRacle attenuated total reflectance (ATR) accessory (Pike Technologies, Wisconsin, USA) and a DTGS (deuterated triglycine sulfate) detector. The spectra were recorded in wavenumber ranges of 650–4000 cm^{-1} by coadding 32 scans at a resolution of 4 cm^{-1}.

The crystallinity indices

X-ray diffraction (XRD) patterns of BSs and DBFs were determined on a MAC science MXP18 instrument (Japan) using Ni-filtered Cu$K_{\alpha 1}$ radiation (λ = 0.1542 nm) at 40 kV and 30 mA. The 2θ range and scan rate were 4–40° and 2°/min, respectively. The crystallinity index (CrI) was calculated according to the equation:

$$CrI = (I_{200} - I_{am})/I_{200} \quad (1)$$

where I_{200} is the intensity of the 200 lattice reflection at 2θ = 22° and I_{am} is the intensity of diffraction of the amorphous material at 2θ = 18.3°.

Thermal stability

The thermal properties of BSs and DBFs were investigated by a Perkin Elmer Pyris 1 instrument (Shelton, CT, USA) through thermogravimetric (TG) analysis. A total of 3 mg of a sample was heated from 50 to 600 °C at constant heating rates of 10 °C/min in a nitrogen atmosphere (20 ml/min).

Fiber morphology

The morphology of DBFs was obtained from scanning electronic microscopy (SEM) micrographs using a JEOL JSM6330F SEM (Tokyo, Japan) with a field emission gun and an acceleration voltage of 3.0 kV. Before testing, all samples were dried and sputtered with platinum.

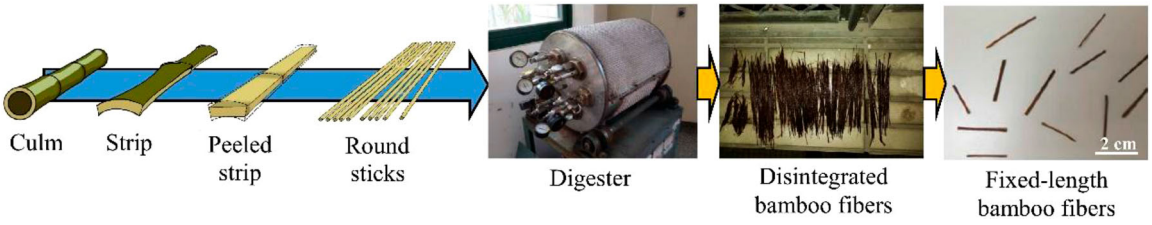

Figure 1. Manufacturing process of disintegrated bamboo fibers.

Tensile testing of disintegrated bamboo fiber

The DBFs were attached to paper with epoxy adhesive in order to clamp with wedge grips. The tensile strength (TS) and tensile modulus (TM) of a DBF were evaluated at a span of 15 mm and a tensile speed of 20 mm/min. The diameters of DBFs were measured using an optical microscope (Olympus BX53M, Olympus Ltd.). Prior to tensile testing, the DBFs were conditioned at 20 °C and 65% relative humidity (RH) for 14 days.

Properties of BCCs

Apparent density of BCCs

After curing for 28 days, the volume of the specimens (size: 50 mm × 50 mm × 50 mm) was measured. Meanwhile, the weight of the specimens was determined to calculate the apparent density (ρ) by the following equation:

$$\rho = m/V \quad (2)$$

where m is the weight of the specimen and V is the volume of the specimen.

Drying shrinkage for BCCs

The shrinkage tests were carried out following the procedure described in CNS 11056 (2005). The test specimens were square prisms with dimensions of 25 mm × 25 mm × 285 mm. After moist curing, the specimens were demolded and kept in a dry environment (25 °C and 80% RH). The shrinkages were measured after 7 and 28 days using a digital length comparator (HCH–129, Jin Ching Her., Co., Ltd., Taiwan). The drying shrinkage values of the BCCs with different DBF contents were calculated as.

$$\text{Drying shrinkage} = (L_x - L_o)/L_{ref} \quad (3)$$

where L_x is the length of the specimen at drying time x (mm), L_o is the length of the specimen before drying (mm), and L_{ref} is the length of the reference (= 250 mm).

Mechanical properties of BCCs

The tensile properties, including the tensile strength (TS) and the tensile modulus (TM), were assessed with a loading speed of 5 mm/min and span of 75 mm according to ASTM C307-18 (2018). The flexural properties, modulus of rupture (MOR) and modulus of elasticity (MOE), were obtained using a three-point static flexural test (sample size: 40 mm × 40 mm × 160 mm) at a flexural speed of 1 kgf/cm^2/sec and a support length of 120 mm according to ASTM C348-21 (2021). The compressive strength (CS) and compressive modulus (CM) were determined using cube specimens with dimensions of 50 mm × 50 mm × 50 mm at a tensile speed of 3 kgf/cm^2/sec according to CNS 1010 (2005).

Specific energy for BCCs

The specific energy (SE) of the BCCs with different DBF contents after various mechanical tests were calculated by the following equation:

$$\text{SE} = \text{Absorbed energy}/(ab) \quad (4)$$

where absorbed energy is the enveloped area of the load – displacement curve after various mechanical tests (tensile, flexural, and compressive tests) from the start of elastic behavior to a reduction in the carrying capacity to 50% of the ultimate load, and a and b are the thickness and width of the specimen.

Morphology of the fracture surface for BCCs

The fracture cross-sectional surfaces of the BCCs were photographed by a smartphone camera (ASUS ZenFone 8, ASUSTek Computer Inc., Taiwan). Its resolution and aperture ratio were 4032 × 3024 pixels and f/2.2, respectively. To observe the fiber distribution in the cement matrix, the color saturation and color temperature for all the pictures were adjusted to 300% and 4396 K, respectively. For failure modes under compressive loading, individual images were recorded by a CMOS (complementary metal–oxide semiconductor) camera (GS3-U3 51S5M-C, Flir Systems, Inc., Canada) with a Computar M7528-MP (New York, USA) lens (a focal length of 75 mm and maximum aperture ratio of f/2.8). The deformation of a specimen surface was photographed at a frame rate of 0.2 Hz during compressive loading and streamed using Point Grey FlyCapture2 (USA). The full-field strain contour employing Gaussian filtering and a filter size of 15 was used by Vic-2D DIC Analysis Software (Correlated Solutions, Inc., Canada).

Analysis of variance

All of the results are expressed as the mean ± standard deviation (SD). The significance of the differences was calculated by Scheffe's test, and p values < 0.05 were considered significant.

Results and discussion

Characteristics of bamboo fibers

As shown in Figure 2, the functional groups of BSs and DBFs were characterized by an FTIR spectrometer to estimate the efficiency of alkali treatment. To compare the spectra of BSs and DBFs, the intensities of all spectra were normalized at 2898 cm^{-1}, which corresponds to C – H stretching in CH_2

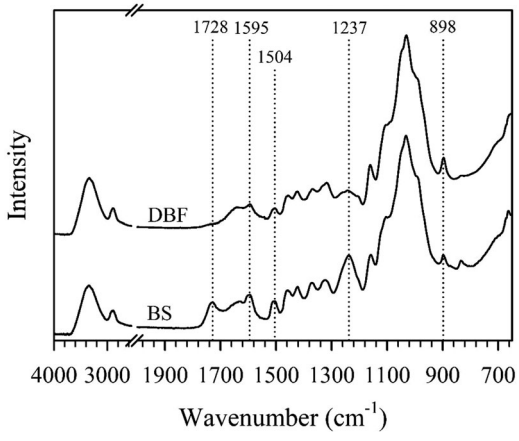

Figure 2. FTIR spectra of the bamboo stick (BS) and disintegrated bamboo fiber (DBF).

and CH_3 (Das and Chakraborty 2006). For the spectrum of the BSs, the band at 1728cm^{-1} was assigned to the stretching of the carbonyl groups (C = O) of acetyls in hemicellulose. This band intensity of the DBFs obviously disappeared after alkali treatment, indicating that alkali treatment causes the removal of hemicellulose. The other characteristic bands of aromatic ring stretching in lignin appeared at 1595 and 1504 cm^{-1} for BSs. In addition, a band appeared at 1237 cm^{-1}, which corresponds to C – C, C – O, and C = O stretching in lignin and xylan. These peak intensities for the DBFs significantly decreased. This finding revealed that the hemicellulose and lignin of bamboo effectively decompose during alkali treatment. Furthermore, after alkali treatment, we noted that the spectrum for the DBFs has an increase in the intensity at 898 cm^{-1}, which corresponds to the asymmetric out-of-plane ring stretching in cellulose. This was attributed to the fact that the relative percentage of cellulose increased due to the degradation of hemicellulose and lignin. Similar results were reported by several researchers (Das and Chakraborty 2006, Chattopadhyay et al. 2011, Li et al. 2017, Lin et al. 2018).

Figure 3 shows the XRD patterns and crystallinity indices (CrIs) of BSs and DBFs. For the BS sample, a small diffraction peak of cellulose crystallographic form was observed at 34.6° (040 lattice plane), while two noticeable peaks were observed at 15.6° (110/10 lattice planes) and 22° (200 lattice plane). In addition, the amorphous region was at 18.3°. The diffraction for untreated bamboo, which corresponds to the preferred orientation along the fiber axis in cellulose I, was reported by previous studies (Liu and Hu 2008, Chen et al. 2017, Yang and Lee 2018, Yeh and Yang 2020, Chen et al. 2021). For DBFs, these characteristic peaks were not significantly different from those of the BSs, implying a similar cellulose structure. This result indicated that the peak positions of bamboo were not influenced by alkali treatment in the present study. However, the CrI of the BSs decreased from 58.6% (DBF) to 48.0%. The reduction in the CrI of alkali-treated BSs (DBFs) may be related to partial lattice transformation from cellulose I to cellulose II. Previous studies reported that alkali treatment led to different lattice transformations in natural fibers (Ishikura et al. 2010, Kobayashi et al. 2011, Nakano and Nakano 2014, Cai et al. 2015, Chen et al. 2021).

Figure 4 illustrates the residual weight (RW) and differential RW curves of BSs and BDFs from the results of the TG analysis to evaluate their thermal stability. As shown in Figure 4a, all RW curves slightly decreased at temperatures from 50 – 120 °C due to water evaporation. In the range of 200 – 370 °C, significant weight loss was observed for all curves since hemicellulose and cellulose completely decomposed, and the partial decomposition of lignin occurred. With a temperature range of 370 – 600 °C, the RW curves for all specimens gently decreased and flattened. This is related to the combustion of the residues, such as the remaining lignin combusted. Additionally, the temperatures at 5% of weight loss ($T_{5\%}$) were 266 and 284 °C for BSs and DBFs, respectively. The results demonstrated that the DBF exhibited better thermal stability than the BSs since the $T_{5\%}$ for the DBFs was higher. Figure 4b displays the differential RW curves of the BSs and DBFs. For BSs, a significant shoulder was displayed in the range of 240 – 310 °C. Yang et al. (2007) reported that hemicellulose was decomposed by pyrolysis in the range of 220 – 315 °C. However, the curve for the DBFs disappeared in the same temperature range. This result implied that alkali treatment effectively removed hemicellulose in bamboo fibers. The SEM images on the surface and end of the DBFs are shown in Figure 5. It can be observed that parenchyma cells severely collapsed, while the fibers separated to twist. This is likely because the alkali treatment removed hemicellulose and lignin in

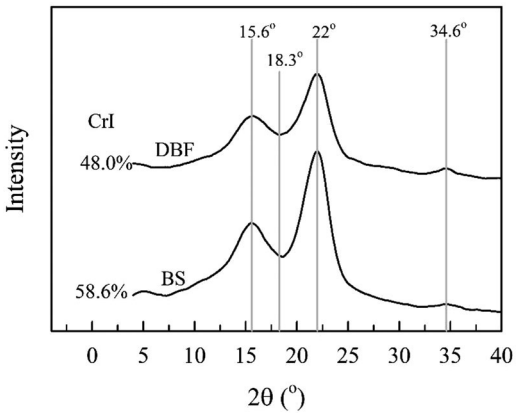

Figure 3. XRD patterns and crystallinity indexes (CrI) of the bamboo stick (BS) and disintegrated bamboo fiber (DBF).

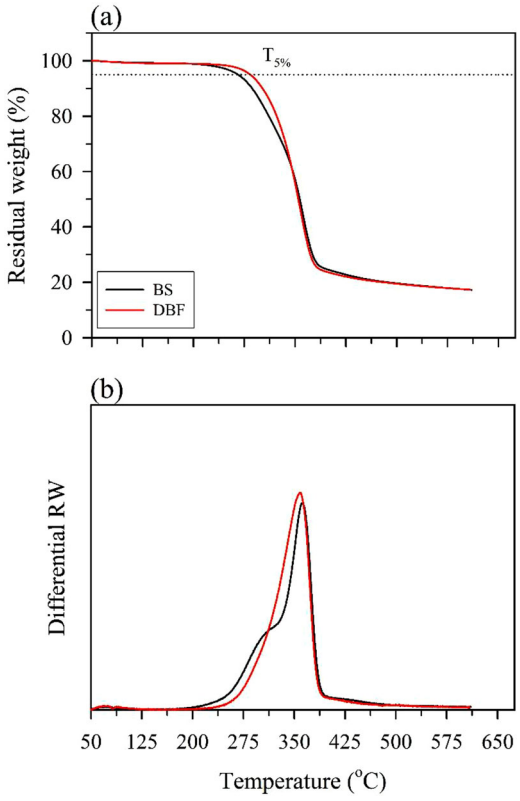

Figure 4. Thermogravimetric curves of the bamboo stick (BS) and disintegrated bamboo fiber (DBF): (a) residual weight (RW) curves; (b) differential RW curves.

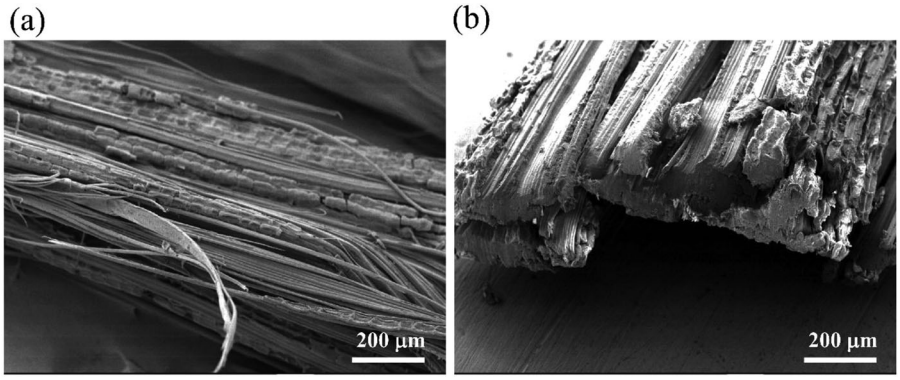

Figure 5. SEM images of the surface: (a) and end (b) of the disintegrated bamboo fiber (DBF).

parenchyma and in the middle lamellae between fibers (Adel Salih et al. 2020, Chen et al. 2021). In this study, the diameter distribution and tensile properties of the DBFs were further investigated (Figure 6). After alkali treatment, the diameter was in the range of 0.1977 – 0.4295 mm (Figure 6a). For the tensile tests of DBFs, the tensile strength (TS) and tensile modulus (TM) range from 117 MPa to 398 MPa and 6 GPa to 21 GPa, respectively. The results are also shown in Table 1. The average diameter, TS, and TM were 0.334 mm, 204 MPa, and 13 GPa, respectively.

Physical and mechanical properties of BCCs

Physical properties

Generally, the density of a material is positively related to its mechanical strength. Additionally, it is well known that cement or concrete undergoes drying shrinkage, which is a spontaneous dimensional variation during drying without any external load. Therefore, the effects of adding DBF content on the apparent density (Table 1) and drying shrinkage (Figure 7) of the DBF/cement composite (BCC) were investigated in this study. As shown in Table 2, the average apparent density (ρ) of the composite without DBFs (BCC0) was 2090kg/m^3. When the DBF content was added to 1 wt% (BCC1), there was no significant difference compared to the ρ value of BCC0. On the other hand, the ρ value of the BCC significantly decreased from 2086kg/m^3 to 1906kg/m^3 as the DBF content was increased from 1 wt% (BCC1) to 3 wt% (BCC3). The results showed that the addition of DBFs to 3 wt% reduced the apparent density of BCC by 8.8% compared to BCC0. The reason for this phenomenon is that the DBFs have a lower density than cement. According to previous studies (Li et al. 2006, Andiç-Çakir et al. 2014, Xie et al. 2015), the increase in the natural fiber content in the cement matrix results in an increase in the porosity of the cementitious composite, causing a decrease in its apparent density. Figure 7 shows the drying shrinkage of the BCCs with different DBF contents. The drying shrinkage of BCC0 was 0.0897% after 7 days

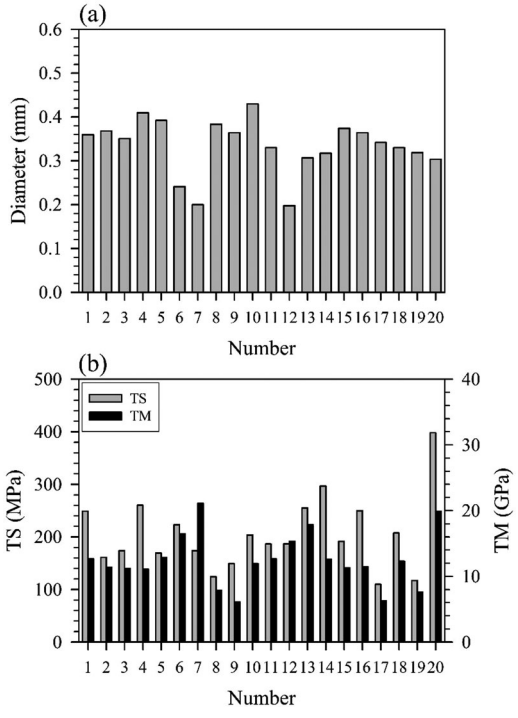

Figure 6. Diameters and tensile properties of the DBFs: (a) diameter; (b) tensile strength (TS) and tensile modulus (TM).

Table 1. The diameter and tensile properties of DBFs.

	Diameter (mm)	TS (MPa)	TM (GPa)
DBF	0.334 ± 0.062	204 ± 68	13 ± 4

Values are mean ± SD (n = 20).

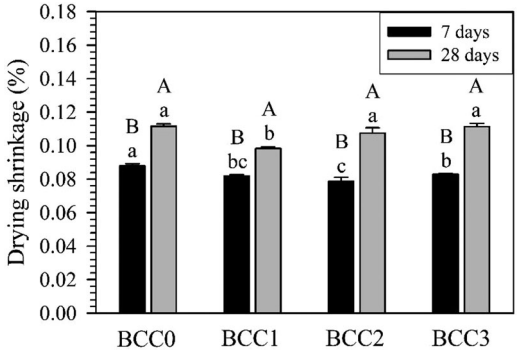

Figure 7. Drying shrinkage of the BCC with different DBF content. Bars with capital letters indicate significant differences among curing times ($p < 0.05$). Bars with lowercase letters indicate significant differences among the BCCs with various DBF content ($p < 0.05$).

Table 2. The mechanical properties and specific energies of the BCCs with different DBF contents.

		Tensile properties			Flexural properties			Compressive properties		
Code	ρ (kg/m^3)	TS (MPa)	TM (GPa)	SE$_t$ (kJ/m^2)	MOR (MPa)	MOE (GPa)	SE$_b$ (kJ/m^2)	CS (MPa)	CM (GPa)	SE$_c$ (kJ/m^2)
BCC0	2090 ± 16^a	4.02 ± 0.12^a	0.32 ± 0.01^a	2.05 ± 0.10^{ab}	6.88 ± 0.59^a	1.63 ± 0.07^a	0.24 ± 0.03^a	23.60 ± 0.93^a	1.15 ± 0.02^a	34.58 ± 0.18^a
BCC1	2086 ± 9^a	4.07 ± 0.11^a	0.26 ± 0.01^b	2.45 ± 0.15^a	6.38 ± 0.30^a	0.93 ± 0.37^a	0.35 ± 0.09^a	24.01 ± 0.70^a	1.22 ± 0.04^a	41.53 ± 4.27^a
BCC2	2001 ± 29^b	3.36 ± 0.25^b	0.20 ± 0.00^c	2.20 ± 0.15^{ab}	5.96 ± 0.12^a	1.37 ± 0.51^a	0.23 ± 0.06^a	17.02 ± 0.42^b	1.42 ± 0.12^a	35.96 ± 9.72^a
BCC3	1906 ± 13^c	2.58 ± 0.21^c	0.15 ± 0.01^d	1.63 ± 0.28^b	4.30 ± 0.07^b	0.80 ± 0.23^a	0.30 ± 0.09^a	13.04 ± 1.26^c	1.29 ± 0.18^a	19.06 ± 0.96^b

Values are mean ± SD (n = 3). Different letters within a column indicate significant differences among the BCCs with various DBF content (p < 0.05).

of curing. When the curing time reached 28 days, the drying shrinkage of BCC0 significantly increased to 0.1116%. An increase in the drying shrinkage of the cement is due to the reduction of the relative humidity in the pores by water evaporation, leading to the occurrence of drying shrinkage and its increase over time (Guo et al. 2020). For the BCC, the drying shrinkage at 7 days of curing time decreased to 0.0787% as the DBF content increased to 2 wt%. When the DBF content was 3 wt%, the drying shrinkage increased to 0.0829%. Similarly, the BCC with 1 wt% DBFs exhibited lower drying shrinkage at 28 days of curing time. The drying shrinkage significantly increased for BCC2; however, there was no significant difference between BCC0 and BCC3. The results indicated that BCCs with DBFs had lower drying shrinkage at the initial stage (7 days) than BCC0. After 28 days of curing, there was no significant difference between BCC0 and BCC with DBF contents above 1 wt%. Furthermore, the change rates of shrinkage from 7 days to 28 days of curing time were 27.0%, 20.0%, 36.6%, and 34.3% for BCC0, BCC1, BCC2, and BCC3, respectively. These results explained that the greater the DBF content in the BCC, the greater the rate of shrinkage changes. This is attributed to the fact that an increase in the DBF content causes an increase in the porosity, including the porosity of the bamboo fibers and the porosity between the fibers and matrix, further facilitating water evaporation in the pores to increase the shrinkage (Bederina et al. 2007, 2012, Guo et al. 2020).

Mechanical properties

To understand the effects of adding DBF content on the tensile properties of the BCCs, a tensile test was carried out to measure the tensile strength and tensile modulus. Figure 8 presents the tensile stress – strain curves of the BCCs with different DBF contents. The curve of the BCC without DBF (BCC0) rapidly decreased after the ultimate stress, indicating that BCC0 is a brittle material under tensile testing. Additionally, brittle failure for all curves of BCCs with different DBF contents was also found. The results implied that BCCs showed the same trend as BCC0 regardless of the DBF content. As shown in Table 2, the tensile strength (TS) and tensile modulus (TM) of BCC0 were 4.02 MPa and 0.32 GPa, respectively. When the DBF content was 1 wt% (BCC1), the TM value significantly decreased. However, there was no significant difference for the TS value. For the BCC with a 3 wt% DBF content (BCC3), the TS and TM values decreased by 35.8% and 53.1%, respectively. This result indicated that the TS and TM values of the BCCs decreased with increasing DBF content above 1 wt%. Figure 9 illustrates the failure cross-sectional surfaces of the BCCs with different DBF contents after the tensile test. As the DBF content increased from 1 wt% to 3 wt%, fiber agglomeration was obviously observed. Therefore, the reduction in the tensile properties can be related to fiber agglomeration (Figure 9) and lower apparent density (Table 1). Furthermore, the absorbed fracture energy of a cement or concrete is one of the important parameters to evaluate the impact strength and the required energy for crack formation (Köksal et al. 2013, Xie et al. 2019). As described in Table 2, the specific energy under tensile test (SE$_t$) of BCC0 is 2.05 kJ/m^2. The SE$_t$ slightly increased to 2.45 kJ/m^2, when the DBF content was 1 wt% (BCC1). With the addition of DBF content to 3 wt% (BCC3), the SE$_t$ significantly decreased to 1.63 kJ/m^2.

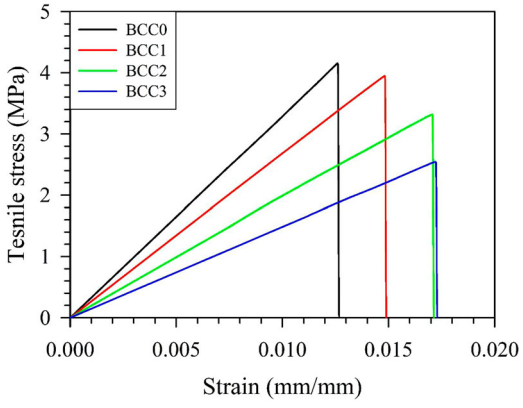

Figure 8. The tensile stress – strain curves of the BCCs with different DBF content.

Figure 10 shows the flexural stress – strain curves of BCCs with different DBF contents. The strain at the ultimate stress of BCC0 is low compared to that of BCCs with DBFs. When DBFs were added into the cement matrix, the higher strain at the ultimate stress of the BCC was due to the DBFs. Additionally, the curves for the BCCs with various DBF contents obviously exhibited gradual failure after the ultimate stress, representing strain softening. The results indicated that the mechanical behavior of the pure cement (BCC0) was brittle fracture, while the BCCs with DBFs showed quasi-brittleness. Therefore, DBFs were effective in restricting the crack propagation and played a role as the bridge of the extended cracks after the ultimate stress (Cao et al. 2019). According to previous studies (Marcalikova et al. 2019, 2020, Cajka et al. 2020), the fiber type and content are important factors affecting the fracture parameters on the stress – strain curves of cementitious composites. In Table 2, BCC0 exhibited flexural properties with MOR and MOE values of 6.88 MPa and 1.63 GPa, respectively. The MOR of the BCCs showed no significant difference when the DBF content reached 2 wt%, at which point it significantly reduced to 4.30 MPa when the DBF content was more than 2 wt%.

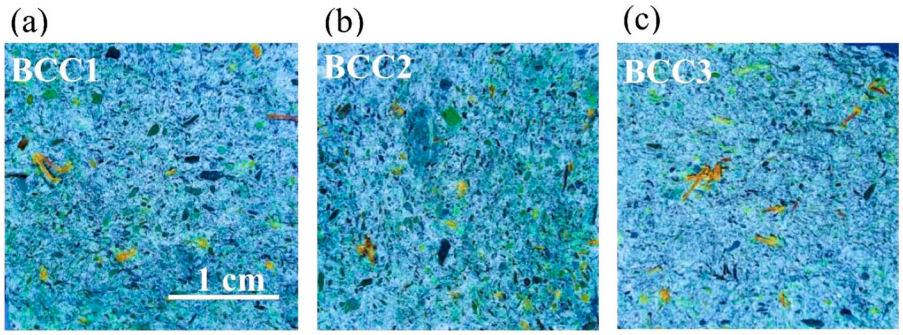

Figure 9. The failure cross-sectional surfaces of the BCCs with different DBF content after the tensile test. The brown areas are fibers.

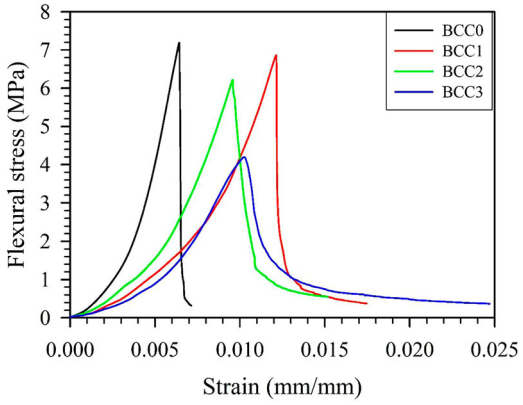

Figure 10. The flexural stress – strain curves of the BCCs with different DBF content.

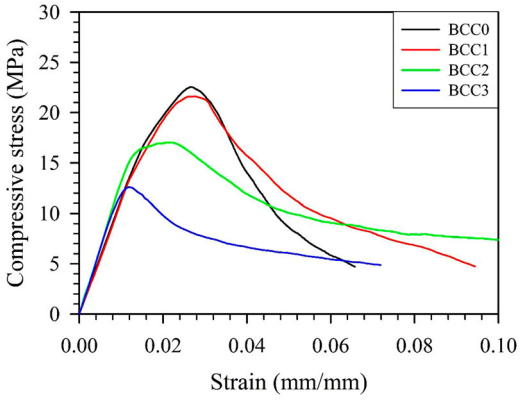

Figure 11. The compressive stress – strain curves of the BCCs with different DBF content.

However, the MOE for all samples ranged from 0.80–1.63 GPa, and there were no significant differences in the MOE values among all samples. The decrease in the MOR of the BCC with higher DBF content is related to the agglomeration and nonuniform mixing of fibers in the cement matrix. Furthermore, the flexural toughness of BCC was also characterized in terms of the specific energy under the bending test (SE_b). The statistical analysis indicated that SE_b had no significant differences between the BCCs with various DBF contents in the range of 0.23–0.35 kJ/m^2.

For compressive properties, Figure 11 depicts the compressive stress – strain curves with various DBF loadings for the BCCs. All of the samples showed similar curves and strain softening in the curves after ultimate stress regardless of the DBF content varying from 0 to 3 wt%. To evaluate the effect of the DBF content on the compressive properties of the BCCs, the compressive strength (CS), compressive modulus (CM), and specific energy under a compression test (SE_c) were further investigated. As shown in Table 2, the CS, CM, and SE_c of BCC0 were 23.60 MPa, 1.15 GPa, and 34.58 kJ/m^2, respectively. When DBFs were added to the cement, these values were not significantly different from those of BCC0. As the DBF content increased from 1 to 3 wt %, the CS significantly decreased from 24.01–13.04 MPa. Additionally, the SE_c was reduced by 44.9% compared to BCC0, when the DBF content increased to 3 wt%. The results indicated that the CS of the BCC has the same tendency as the TS and MOR. In addition to the causes of

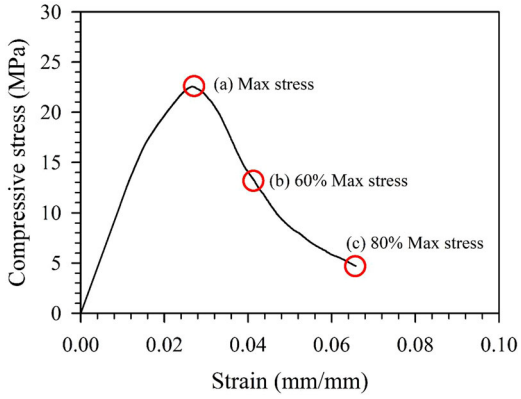

Figure 12. Positions showing failure modes on the compressive stress – strain curve of the specimen at different stress levels.

nonuniform mixing and fiber agglomeration, Bentchikou et al. (2012) reported that the porosity in the cement matrix increases with increasing fiber content, resulting in BCC forming a light and fragile material. The failure modes of the BCCs at different stress levels are presented in Figures 12 and 13, respectively. The failure mode of BCC0 and BCC1 showed a nonexplosive and shear failure mode after ultimate stress. However, the BCCs illustrated more than one longitudinal crack on the surface of the specimens when the DBF content was above 1 wt% (BCC2 and BCC3). Xie et al. (2020) reported that multiple longitudinal cracks were formed

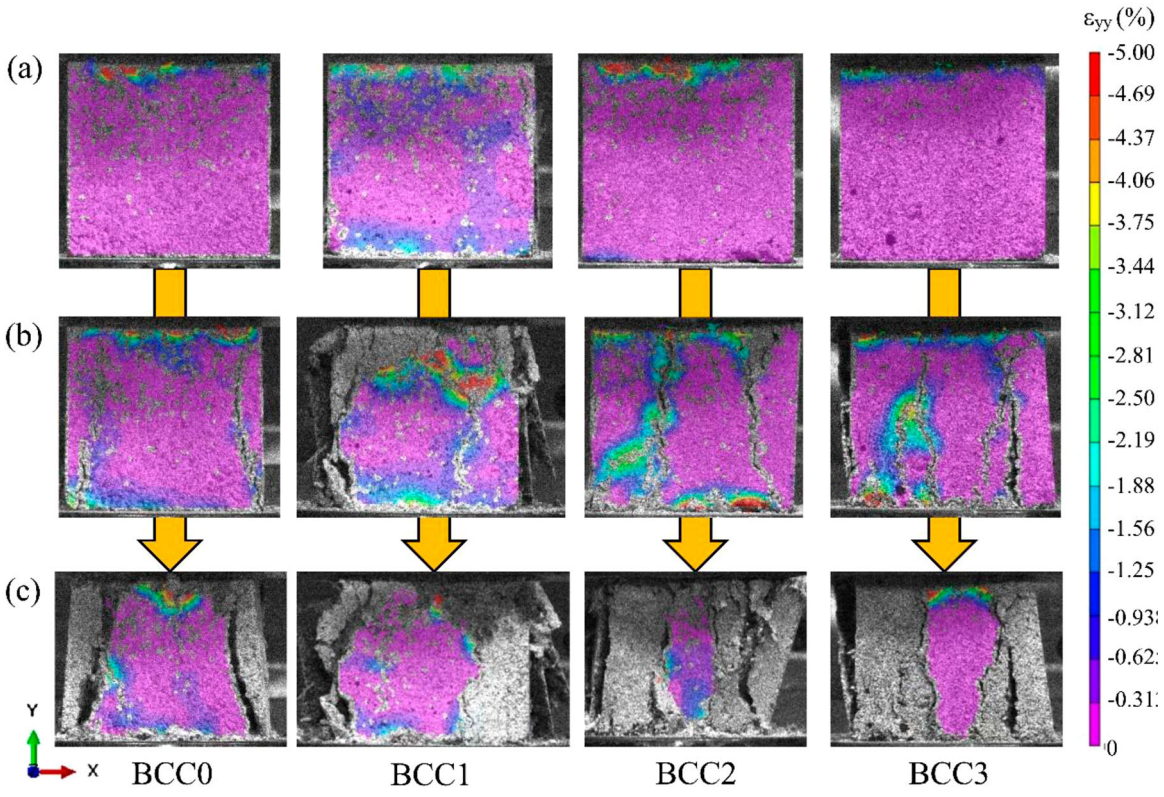

Figure 13. Sequences of compressive failure modes on the surface of the specimens at different stress levels: (a) max stress; (b) 60% of max stress; (c) 80% of max stress.

under uniaxial compressive loading since the fibers can significantly transfer stress in various directions due to their random and three-dimensional distribution in the cement matrix.

Conclusions

In this study, DBFs were extracted from alkali-treated makino BSs and were added into a cement matrix to fabricate bamboo fiber/cementitious composites (BCCs). Regarding the functional groups of DBFs using FTIR, hemicellulose and lignin effectively decomposed after alkali treatment, while the relative percentage of cellulose increased. In addition, the crystallinity index of the DBFs calculated from the XRD pattern was lower than that of the BSs due to partial lattice transformation of cellulose. Due to the removal of hemicellulose, lignin and extractives in bamboo fibers, the DBFs exhibited better thermal stability than the BSs. The SEM images demonstrated the collapse of parenchyma cells and separation and twist of the fibers. The diameter, tensile strength, and tensile modulus of the DBFs were in the ranges of 0.1977 – 0.4295 mm, 117 – 398 MPa, and 6 – 21 GPa, respectively. When the addition of DBFs increased above 1 wt%, most of the physico-mechanical properties significantly decreased with increasing DBF content, including the density, tensile properties, flexural properties, and compressive properties. For drying shrinkage, BCC with 1 wt% of DBFs exhibited the lowest shrinkage at 28 days of curing time. However, the specific energy under the tensile test of the BCC with 1 wt% DBFs slightly increased, while there were no significant differences with the pure cement for the specific energies under the flexural test and compressive test. For the failure mode, more than one longitudinal crack was observed on the surfaces of the BCCs as the DBF content increased above 1 wt%. As described above, the optimal DBF content was 1 wt% in the BCC. These results indicated that alkali treatment changed the functional groups, crystallinity, and thermal stability of the bamboo fibers, and the addition of DBFs significantly affected the physical and mechanical properties of BCCs.

Acknowledgements

This work was financially supported by a research grant from the Ministry of Science and Technology, Taiwan (MOST 108-2313-B-005-014-MY3). We thank the Instrument Center of National Chung Hsing University for help with measurements of XRD patterns (MOST 110-2731-M-005-001-).

Disclosure statement

No potential conflict of interest was reported by the author(s).

Funding

This work was supported by Ministry of Science and Technology (MOST), Taiwan: [Grant Number MOST 108-2313-B-005-014-MY3].

ORCID

Teng-Chun Yang http://orcid.org/0000-0001-7291-5419
Hsuan-Teh Hu http://orcid.org/0000-0001-8582-0670

References

Adel Salih, A., Zulkifli, R. and Azhari, C. H. (2020) Tensile properties and microstructure of single-cellulosic bamboo fiber strips after alkali treatment. *Fibers*, *8*, 26. doi:10.3390/fib8050026

Andiç-Çakir, Ö, Sarikanat, M., Tüfekçi, H. B., Demirci, C. and Erdoğan, ÜH (2014) Physical and mechanical properties of randomly oriented coir fiber–cementitious composites. *Composites Part B: Engineering*, *61*, 49–54. doi:10.1016/j.compositesb.2014.01.029

ASTM C307-18 (2018) Standard test method for tensile strength of chemical -resistant mortar, grouts, and monolithic surfacings. American Society of Testing and Materials, *06*(02), 1–4. Available at: https://www.astm.org/c0307-18.html

ASTM C348-21 (2021) Standard test method for flexural strength of hydraulic-cement mortars. American Society of Testing and Materials, *04*(01), 1–6. Available at: https://www.astm.org/c0348-21.html

Bederina, M., Gotteicha, M., Belhadj, B., Dheily, R. M., Khenfer, M. M. and Quéneudec, M. (2012) Drying shrinkage studies of wood sand concrete – effect of different wood treatments. *Construction and Building Materials*, *36*, 1066–1075. doi:10.1016/j.conbuildmat.2012.06.010

Bederina, M., Marmoret, L., Mezreb, K., Khenfer, M. M., Bali, A. and Quéneudec, M. (2007) Effect of the addition of wood shavings on thermal conductivity of sand concretes: Experimental study and modelling. *Construction and Building Materials*, *21*, 662–668. doi:10.1016/j.conbuildmat.2005.12.008

Bentchikou, M., Guidoum, A., Scrivener, K., Silhadi, K. and Hanini, M. (2012) Effect of recycled cellulose fibres on the properties of lightweight cement composite matrix. *Construction and Building Materials*, *34*, 451–456. doi:10.1016/j.conbuildmat.2012.02.097

Cai, M., Takagi, H., Nakagaito, A. N., Katoh, M., Ueki, T., Waterhouse, G. I. and Li, Y. (2015) Influence of alkali treatment on internal microstructure and tensile properties of abaca fibers. *Industrial Crops and Products*, *65*, 27–35. doi:10.1016/j.indcrop.2014.11.048

Cajka, R., Marcalikova, Z., Kozielova, M., Mateckova, P. and Sucharda, O. (2020) Experiments on fiber concrete foundation slabs in interaction with the subsoil. *Sustainability*, *12*, 3939. doi:10.3390/su12093939

Cao, M., Xie, C. and Guan, J. (2019) Fracture behavior of cement mortar reinforced by hybrid composite fiber consisting of CaCO3 whiskers and PVA-steel hybrid fibers. *Composites Part A: Applied Science and Manufacturing*, *120*, 172–187. doi:10.1016/j.compositesa.2019.03.002

Chakraborty, S., Kundu, S. P., Roy, A., Adhikari, B. and Majumder, S. B. (2013) Polymer modified jute fibre as reinforcing agent controlling the physical and mechanical characteristics of cement mortar. *Construction and Building Materials*, *49*, 214–222. doi:10.1016/j.conbuildmat.2013.08.025

Chattopadhyay, S. K., Khandal, R. K., Uppaluri, R. and Ghoshal, A. K. (2011) Bamboo fiber reinforced polypropylene composites and their mechanical, thermal, and morphological properties. *Journal of Applied Polymer Science*, *119*, 1619–1626. doi:10.1002/app.32826

Chen, H., Wu, J., Shi, J., Zhang, W. and Wang, H. (2021) Effect of alkali treatment on microstructure and thermal stability of parenchyma cell compared with bamboo fiber. *Industrial Crops and Products*, *164*, 113380. doi:10.1016/j.indcrop.2021.113380

Chen, H., Yu, Y., Zhong, T., Wu, Y., Li, Y., Wu, Z. and Fei, B. (2017) Effect of alkali treatment on microstructure and mechanical properties of individual bamboo fibers. *Cellulose*, *24*, 333–347. doi:10.1007/s10570-016-1116-6

CNS 1010 R3032 (2005) Method of test for compressive strength of hydraulic cement mortars (using 50mm or 2 in. cube specimens) (Chinese). National Standards of the Republic of China, R3032, 1–3.

CNS 11056 A3217 (2005) Method of measuring the drying shrinkage of mortar containing portland cement (Chinese). National Standards of the Republic of China, A3217, 1–3.

CNS 3655 R2079 (2005) Method for mechanical mixing of hydraulic cement pates and mortars of plastic consistency (Chinese). National Standards of the Republic of China, R2079, 1–2.

Das, M. and Chakraborty, D. (2006) Influence of alkali treatment on the fine structure and morphology of bamboo fibers. *Journal of Applied Polymer Science*, *102*, 5050–5056. doi:10.1002/app.25105

Filho, R. D. T., Ghavami, K., Sanjuán, M. A. G. L. and England, G. L. (2005) Free, restrained and drying shrinkage of cement mortar composites reinforced with vegetable fibres. *Cement and Concrete Composites*, *27*, 537–546. doi:10.1016/j.cemconcomp.2004.09.005

Guo, A., Sun, Z. and Satyavolu, J. (2020) Impact of modified kenaf fibers on shrinkage and cracking of cement pastes. *Construction and Building Materials*, *264*, 120230. doi:10.1016/j.conbuildmat.2020.120230

Ishikura, Y., Abe, K. and Yano, H. (2010) Bending properties and cell wall structure of alkali-treated wood. *Cellulose*, *17*, 47–55. doi:10.1007/s10570-009-9360-7

Kobayashi, K., Kimura, S., Togawa, E. and Wada, M. (2011) Crystal transition from Na–cellulose IV to cellulose II monitored using synchrotron X-ray diffraction. *Carbohydrate Polymers*, *83*, 483–488. doi:10.1016/j.carbpol.2010.08.006

Köksal, F., Şahin, Y., Gencel, O. and Yiğit, İ (2013) Fracture energy-based optimisation of steel fibre reinforced concretes. *Engineering Fracture Mechanics*, *107*, 29–37. doi:10.1016/j.engfracmech.2013.04.018

Li, M., Zhou, S. and Guo, X. (2017) Effects of alkali-treated bamboo fibers on the morphology and mechanical properties of oil well cement. *Construction and Building Materials*, *150*, 619–625. doi:10.1016/j.conbuildmat.2017.05.215

Li, Z. J., Wang, L. J. and Wang, X. G. (2006) Flexural characteristics of coir fiber reinforced cementitious composites. *Fibers and Polymers*, *7*, 286–294. doi:10.1007/BF02875686

Li, Z., Wang, X. and Wang, L. (2006) Properties of hemp fibre reinforced concrete composites. *Composites Part A: Applied Science and Manufacturing*, *37*, 497–505. doi:10.1016/j.compositesa.2005.01.032

Lin, J., Yang, Z., Hu, X., Hong, G., Zhang, S. and Song, W. (2018) The effect of alkali treatment on properties of dopamine modification of bamboo fiber/polylactic acid composites. *Polymers*, *10*, 403. doi:10.3390/polym10040403

Liu, Y. and Hu, H. (2008) X-ray diffraction study of bamboo fibers treated with NaOH. *Fibers and Polymers*, *9*, 735–739. doi:10.1007/s12221-008-0115-0

Marcalikova, Z., Cajka, R., Bilek, V., Bujdos, D. and Sucharda, O. (2020) Determination of mechanical characteristics for fiber-reinforced concrete with straight and hooked fibers. *Crystals*, *10*, 545. doi:10.3390/cryst10060545

Marcalikova, Z., Prochazka, L., Pesata, M., Bohacova, J. and Cajka, R. (2019) Comparison of material properties of steel fiber reinforced concrete with two types of steel fiber. *Iop Conference Series: Materials Science and Engineering*, *549*, 1–8. doi:10.1088/1757-899X/549/1/012039

Nakano, S. and Nakano, T. (2014) Change in circularity index of cell lumen in a cross-section of wood induced by aqueous NaOH. *Journal of Wood Science*, *60*, 99–104. doi:10.1007/s10086-013-1382-y

Onésippe, C., Passe-Coutrin, N., Toro, F., Delvasto, S., Bilba, K. and Arsène, M. A. (2010) Sugar cane bagasse fibres reinforced cement composites: Thermal considerations. *Composites Part A: Applied Science and Manufacturing*, *41*, 549–556. doi:10.1016/j.compositesa.2010.01.002

Sanchez-Echeverri, L. A., Ganjian, E., Medina-Perilla, J. A., Quintana, G. C., Sanchez-Toro, J. H. and Tyrer, M. (2021) Mechanical refining combined with chemical treatment for the processing of bamboo fibres to produce efficient cement composites. *Construction and Building Materials*, *269*, 121232. doi:10.1016/j.conbuildmat.2020.121232

Sanchez-Echeverri, L. A., Medina-Perilla, J. A. and Ganjian, E. (2020) Nonconventional Ca(OH)2 treatment of bamboo for the reinforcement of cement composites. *Materials*, *13*, 1892. doi:10.3390/ma13081892

Silva, F. d. A., Filho, R. D. T., Filho, J. d. A. M. and Fairbairn, E. d. M. R. (2010) Physical and mechanical properties of durable sisal fiber–cement composites. *Construction and Building Materials*, *24*, 777–785. doi:10.1016/j.conbuildmat.2009.10.030

Tonoli, G. H. D., Belgacem, M. N., Siqueira, G., Bras, J., Savastano, H. and Rocco, F. A. (2013) Processing and dimensional changes of cement based composites reinforced with surface-treated cellulose fibres. *Cement and Concrete Composites*, *37*, 68–75. doi:10.1016/j.cemconcomp.2012.12.004

Xie, C., Cao, M., Si, W. and Khan, M. (2020) Experimental evaluation on fiber distribution characteristics and mechanical properties of calcium carbonate whisker modified hybrid fibers reinforced cementitious composites. *Construction and Building Materials*, *265*, 120292. doi:10.1016/j.conbuildmat.2020.120292

Xie, X., Zhou, Z., Jiang, M., Xu, X., Wang, Z. and Hui, D. (2015) Cellulosic fibers from rice straw and bamboo used as reinforcement of cement-based composites for remarkably improving mechanical properties. *Composites Part B: Engineering*, *78*, 153–161. doi:10.1016/j.compositesb.2015.03.086

Xie, X., Zhou, Z. and Yan, Y. (2019) Flexural properties and impact behaviour analysis of bamboo cellulosic fibers filled cement based composites. *Construction and Building Materials*, *220*, 403–414. doi:10.1016/j.conbuildmat.2019.06.029

Yang, H., Yan, R., Chen, H., Lee, D. H. and Zheng, C. (2007) Characteristics of hemicellulose, cellulose and lignin pyrolysis. *Fuel*, *86*, 1781–1788. doi:10.1016/j.fuel.2006.12.013

Yang, T.-C. and Lee, T.-Y. (2018) Effects of density and heat treatment on the physico-mechanical properties of unidirectional round bamboo stick boards (UBSBs) made of makino bamboo (*phyllostachys makinoi*). *Construction and Building Materials*, *187*, 406–413. doi:10.1016/j.conbuildmat.2018.07.182

Yeh, C.-H. and Yang, T.-C. (2020) Utilization of waste bamboo fibers in thermoplastic composites: Influence of the chemical composition and thermal decomposition behavior. *Polymers*, *12*, 636. doi:10.3390/polym12030636

Zhou, X. M., Ghaffar, S. H., Dong, W., Oladiran, O. and Fan, M. (2013) Fracture and impact properties of short discrete jute fibre-reinforced cementitious composites. *Materials & Design*, *49*, 35–47. doi:10.1016/j.matdes.2013.01.029